HHS Public Access

Author manuscript

Curr Osteoporos Rep. Author manuscript; available in PMC 2019 February 01.

Published in final edited form as:

Curr Osteoporos Rep. 2018 February ; 16(1): 32–41. doi:10.1007/s11914-018-0414-3.

Solute Transport in the Bone Lacunar-Canalicular System (LCS)

Liyun Wang, Ph.D.

Center for Biomechanical Research, Department of Mechanical Engineering, University of Delaware, 130 Academy Street, Newark, DE 19716, 302-831-2659 (office), lywang@udel.edu

Abstract

Purpose of review—Solute transport in the lacunar-canalicular system (LCS) plays important roles in osteocyte metabolism and cell-cell signaling. This review will summarize recent studies that establish pericellular matrix (PCM), discovered inside the LCS, as a crucial regulator of solute transport in bone.

Recent findings—Utilizing confocal imaging and mathematical modeling, recent studies successfully quantified molecular diffusion and convection in the LCS as well as the size-dependent sieving effects of the PCM, leading to the quantification of the effective PCM fiber spacing (10 to 17 nm) in murine adult bones. Perlecan/HSPG2, a large linear proteoglycan, was identified to be an essential PCM component.

Summary—The PCM-filled LCS is bone's chromatographic column, where fluid/solute transport to and from the osteocytes is regulated. The chemical composition, deposition rate and turnover rate of the osteocyte PCM should be further defined to better understand osteocyte physiology and bone metabolism.

Keywords

Osteocyte; lacunar-canalicular system; solute diffusion and convection; pericellular matrix; molecular sieving; perlecan

INTRODUCTION

1.1 Osteocytes' roles in bone and beyond

Osteocytes, the terminally differentiated cells in the osteogenic lineage, are the most abundant bone cells, constituting over 90% of the total bone cell population [1, 2]. Previously, osteocytes were perceived as "passive placeholders" during their long lifespan (up to decades) after retiring from being bone-forming osteoblasts and becoming embedded in mineralized matrix [1]. Nevertheless, the viability of osteocytes has long been deemed important to bone health based on the observation of extensive osteocyte apoptosis associated with osteonecrosis [3], the occurrence of micropetrosis (*i.e.*, mineral refilling of the osteocyte lacunae and canaliculi) following osteocyte death [4], and the increasing number of empty lacunae found in aged and fractured bones [5]. Earlier studies on transport phenomena in bone were driven primarily by the desire of understanding how osteocytes

Disclosure: No potential conflicts of interest relevant to this article were reported.

survive in the mineralized matrix, which is a significant barrier for nutrient supplies and waste removal [6, 7].

Groundbreaking findings during the past three decades have led to a conceptual paradigm shift regarding osteocytes. No longer being viewed as “passive placeholders”, osteocytes are believed to serve as primary mechanical sensors that actively monitor the health of bone matrix [1]. They secrete a multitude of signaling molecules including sclerostin, RANKL (Receptor activator of nuclear nactor kappa-B ligand), OPG (Osteoprotegerin), NO (Nitric oxide), and PGE_2 (Prostaglandin E_2), through which osteocytes orchestrate the activities of osteoblasts and osteoclasts during bone remodeling [1]. In fact, sclerostin is an emerging therapeutic target for treating osteoporosis [8]. Furthermore, osteocytes are also found to regulate bone mineralization via DMP1 (Dentin matrix acidic phosphoprotein 1), PHEX (Phosphate regulating endopeptidase homolog, X-linked), and MEPE (Matrix extracellular phosphoglycoprotein) and regulate serum phosphate via endocrine signaling of FGF32 (fibroblast growth factor 23) with distant organs beyond bones (see reviews [1, 2, 9]). Since most of these osteocyte-derived signaling molecules have to travel through the bone matrix before reaching their target cells and organs, solute transport in bone is thus highly relevant in this context.

1.2. Factors impacting osteocytes’ viability

As the long-lived cells entombed in calcified matrix [10], osteocytes depend on nutrient supply and waste removal, a dynamic transport process operating between the cells and the vasculature, for their survival [7]. Although diffusion through mineralized matrix may be adequate for the transport of small molecules, Piekarski and Munro (1977) argued that transport of large molecules requires convection induced by mechanical loading to augment the limited diffusion as shown in their theoretical modeling [6]. Later studies identified some large molecules produced by osteocytes, including sclerostin (24k Da) [11] and RANKL (20kDa) [12–14]. In addition to enhancing solute transport, physiological mechanical loading associated with exercise and locomotion has been shown to impart powerful beneficial effects on osteocytes’ viability *in vitro* and *in vivo*, possibly through activation of wnt/β-catenin [15], PKA (Protein kinase A) [16], and other signaling pathways [17, 18]. Extensive studies have established that, among various types of load-induced stimulations (such as matrix deformation, hydraulic pore pressure, streaming potential, and interstitial fluid flow), interstitial fluid flow may be the primary physical signal which osteocytes sense and respond to [7, 19, 20].

1.3. LCS as the main conduit for fluid and solute transport around osteocytes

The hierarchical structure of various pores in bone matrix has been revealed and analyzed using a wide range of imaging and bioengineering approaches [21]. The three porosity levels (reviewed in [22]) vary greatly in size, from vascular pores associated with the Haversian canals (order 10–50 μm), the lacunar-canalicular system (LCS) housing osteocyte cell body and dendrites (order 0.1–1 μm), to the microscopic pores associated with collagen-hydroxyapatite (order 10 nm). Transport within these inter-connecting pores is relevant to the functions of osteoblasts and osteoclasts (close to the vasculature), osteocytes (enclosed in LCS), as well as the hydration and mechanical properties of the extracellular matrix

(depending on intra- and inter-collagen hydration), respectively. In this short review, we will focus on transport at the osteocyte LCS level. Reviews on transport at the other two porosity levels can be found in literature [21, 23, 24].

The importance of fluid flow in the LCS was first hypothesized by E.H. Burger and coworkers based on the robust responses of osteocytes in response to fluid flow *in vitro* [25]. However, at that time this new concept of fluid flow inside LCS seemed incompatible with the existing experimental streaming potential measurement, an indirect indicator of fluid flow over charged bone surface. From the relaxation time of streaming potentials under step loading, fluid was predicted to flow through the microscopic pores (order 10 nm) in the bone matrix [26]. In contrast, fluid flow through the canalicular channel was predicted to relax 1000 times faster [19]. A breakthrough was made by Weinbaum, Cowin, and coworkers [19, 27, 28], where a gel-like pericellular fiber matrix with a fiber spacing of 7 nm (the size of albumin) was proposed to fill the fluid flow pathway in the LCS. Predictions of their models agreed very well with various experimental measurements of streaming potentials, eventually leading to the general acceptance that the origin of bone fluid flow is within the LCS (reviewed in [22], [7]). With more detailed experimental data on the LCS structure, especially the findings of the tethering fibers [29] and integrin attachments [30], the group developed much more sophisticated models that greatly improve our understanding of the mechanosensing and mechanotransduction in osteocytes [29–31]. Excellent reviews have been published on load-induced fluid flow and bone mechanotransduction [7], in addition to advances in assessing bone porosity and permeability [21, 32].

1.4. Focus of this review

We will summarize recent published data on solute transport in the LCS from both experimental and modeling aspects. With new advances on imaging and modeling, unprecedented new insights on the multi-scale transport phenomena have been achieved. The *in situ* measurements of molecular diffusion and convection, the size-dependent sieving properties of the LCS, and the identification of a key pericellular matrix component (perlecan) in LCS will be summarized in the subsequent sections, followed by discussions of unresolved questions and future directions.

2. SOLUTE TRANSPORT IN THE LCS: IMPACTS OF MOLECULAR SIZE, SHAPE, AND MECHANICAL LOADING

2.1. Molecules of interest

The desire to understand how endogenous factors and exogenous agents move inside bone has driven the investigation of solute transport in the LCS. The endogenous factors of interest include nutrients, hormones, and other bioactive molecules such as cytokines and growth factors, which osteocytes either need for survival, or secrete and/or respond to in various conditions. Osteocytes may also be exposed to exogenous agents that are introduced to treat various bone conditions. These endogenous and exogenous molecules vary greatly in molecular size and weight (from hundreds of Daltons up to a hundred thousand Daltons [33, 34]), including (but not limited to) glucose (180 Da), bisphosphonates (250 Da), estrogen/testosterone (280 Da), PGE_2 (352 Da), Raloxifene® (475 Da), calcitonin (3.4 kDa),

Teriparatide® (4.1 kDa), osteocalcin (5.7 kDa), IGF-1 (Insulin-like growth factor 1, 7.6 kDa), PTH (Parathyroid hormone, 9.5 kDa), PTHrp (Parathyroid hormone-related protein, 18kDa), soluble RANKL (20kDa), IL-6 (Interleukin 6, 21 kDa), sclerostin (24 kDa), TNF-α (Tumor necrosis factor α, 26 kDa), BMP2 (Bone morphogenetic protein 2, 26 kDa), TGF-β (Transforming growth gactor β, 44 kDa), MMP-13 (Matrix metallopeptidase 13, 54 kDa), OPG (60 kDa), Denosumab® (145 kDa), and Romosozumab® (145 kDa). The times for these molecules to penetrate into bone tissue and to be cleared from the tissue are important in our understanding of osteocyte physiology, bone metabolism, and drug delivery.

2.2. Molecular sieving and the cut-off size

To probe the permeability of LCS to the aforementioned endogenous and exogenous factors, various sized tracers ranging from small molecules to large proteins and dextrans have been injected to the blood stream *in vivo* or perfused into bone slices *in vitro*, and their deposition and distribution inside bone matrix were tracked either in intact bone or histological sections (reviewed in [7]). These experimental data have clearly demonstrated that the LCS behaves as a molecular sieve: tracers with increasing molecular weights could leak out of vasculature and penetrate into LCS at decreasing rates until the molecules become too big to pass. Selective recent *in vivo* perfusion studies with various sized tracers and their results (tracer penetration to LCS, diffusivity and the characteristic diffusion time over an osteon) are summarized in Table 1. Please note that most results listed in Table 1 were obtained with *in vivo* tracer perfusion with no mechanical loading applied unless stated otherwise. Clearly, these perfusion studies demonstrate that the cut-off size of the LCS in adult bone lays between 7 and 12 nm, which is consistent with the fiber spacing (10–13 nm) later measured using advanced imaging and molecular sieving modeling [35], as discussed in Section 3.2.

2.3. Size- and shape-dependent molecular diffusion

Although the tracer perfusion studies reviewed above provided information whether a molecule of certain size can or cannot penetrate the bone LCS within a specific time-period, quantitative measurements of solute diffusion in the LCS have been extremely difficult to obtain, mainly due to the small dimensions of the LCS and the mineralization of the surrounding matrix. Earlier studies were performed by monitoring tracer efflux from pre-perfused bone blocks [40, 41], which required hours to complete and tissue deterioration may have confounded the measurements. To overcome these problems, we developed an approach combining the Fluorescence recovery after photobleaching (FRAP) imaging with mathematical modeling, which allowed direct measurements of solute transport in intact bones at the LCS level under a laser scanning confocal microscope with high spatiotemporal resolution and tissue penetration [36]. In this FRAP approach, fluorescent tracer molecules are introduced into bone and then a single lacuna is photobleached under intense laser illumination. Subsequently, the influx of unbleached tracers from neighboring lacunae results in an increase of fluorescence intensity in the photobleached lacuna, which is monitored directly by confocal microscopy. The mobility of the fluorescent molecules is then calculated from the time course of fluorescence recovery, using an anatomically based mathematical model. This method has been successfully applied in quantifying the diffusion of molecules of varying size and shape [33], as well as the convection under blood pressure [42] or mechanical loading [34, 35, 43].

To determine the size- and shape-dependency of molecular diffusion in the bone LCS, diffusivity of various sized globular tracers (sodium fluorescein, parvalbumin, ovalbumin) and linear dextrans of 3 kDa and 10 kDa was measured using FRAP in adult murine tibial LCS [33] (Table 1). Compared with their free diffusion in solution, these tracers all showed significant reduction (>45%) in diffusion within the bone LCS [33], which agreed with the presence of pericellular matrix, a molecular sieve, in the LCS. Diffusivity in the bone LCS decreased with increasing molecular weight for both linear and globular molecules, with the linear dextrans decreasing at a faster rate [33] (Table 1). Despite the permeation of dextran-10k in the bone LCS, recovery after photobleaching was not detected within the recording time (~5 min), suggesting some potential entanglement of the flexible dextran chains with the pericellular matrix.

These quantitative measurements demonstrate the importance of the LCS as a critical lifeline for fully entombed osteocytes. Nutrients (~400 Da like fluorescein) and other signaling molecules (~40 kDa like ovalbumin) can diffuse rapidly in these channels with a characteristic time ($t_c = d^2/D$) from one osteocyte to its neighbors (with a typical distance d = 30 μm) within ~3 to 13 sec, respectively. On the scale of individual osteons with a radius of 150 μm, the characteristic time t_c for the small nutrients and the large signaling molecules would vary from 68 to 346 sec, respectively (Table 1). As shown in the next section, these transport times can be shortened in the presence of mechanical loading.

2.4. Transport enhancement by mechanical loading and vascular pressure

It is well accepted that convection due to mechanical loading augments solute diffusion in bone as demonstrated in theory [6] and observed on histological sections [38, 39, 44]. However, the velocity of solute convection within the LCS was not quantified until the development of the FRAP-based velocimetry method [34, 45]. By performing and comparing paired FRAP experiments on the same bone under both non-loaded and loaded conditions, we could separate diffusion from convection and derive the velocity (convection) of studied molecule in the canaliculi using an anatomically validated transport model [45]. Results from three experimental studies on young and aged mice are summarized in Table 2. In the first study [34], sodium fluorescein was measured to move at a peak velocity of 53.9 μm/s in the canalicular channels located 30–50 μm below the anterior-medial tibial surface that was 30%–40% distal to the tibial proximal end, while the tibia was cyclically loaded at a peak load of 3 N at 0.5 Hz with 4 seconds resting time. This moderate mechanical strain (477 με) resulted in a 31% increase in the overall transport rate over diffusion [34]. Using a larger tracer (parvalbumin, 12.3 kDa), a later study [43] demonstrated that the transport enhancement (convection over diffusion: k/k_0) increased nearly linearly with increasing loading magnitude (0, 2.8 N, 4.8 N, $k/k_0 = 1.0 + 0.107$ Load (N)) and decreases with loading frequency (0.5, 1, and 2 Hz). The observed magnitude-and frequency-dependences of transport enhancement agreed well with our theoretical predictions [45]. The convective velocity of parvalbumin (V_s) was measured to be 43.1, 33.3, 28.5 μm/s for 2.8 N loading at 0.5, 1, and 2 Hz, while the velocity increased to 55.8 μm/s for 4.8 N loading at 0.5 Hz in young adult murine bone (20–22-week-old, Table 2). In the third study on aged (12–13-month-old) mice [35], faster convective velocities of sodium fluorescein and parvalbumin were measured (51.1 and 48.2 μm/s) in tibiae loaded at 2.8 N and 0.5 Hz (Table 2), due to

the decreased density of the pericellular matrix in aged LCS as detailed in the next section [35].

These convection measurements clearly demonstrate the importance of physiological loading in enhancing nutrient supply and cell-cell signaling in bone. Moderate loading (2.8–4.8 N, ~300–500 με surface strain) results in significant transport enhancement (14%–50%) for either small nutrients or signaling molecules of ~10 kDa [34, 35, 43], and the induced convective velocities (28.5–55.8 μm/s) are in the same order of capillary blood flows (~50 μm/s). In the context of molecular exchange within single osteons (radius of 150 μm), the characteristic transport time ($t_C = R_C / V_s$) for small nutrients and 10 kDa signaling molecules in the loaded bone is in the range of 2.7–8.8 sec (Table 2), which is more than 10 times shorter than that due to diffusion only (68–143 sec) listed in Table 1 (Section 2.3).

In addition to mechanical loading, vascular pressure has also been proposed to drive interstitial fluid flow within the LCS and augment solute diffusion in bone [46]. To test this hypothesis, we measured the transport rate of sodium fluorescein within the tibial LCS in anesthetized mice (in the presence of vascular pressure), followed by repeating the measurements at the same locations/lacunae in the same animals after sacrifice (in the absence of vascular pressure) [42]. If vascular pressure indeed induced interstitial fluid flow, the transport rates measured from the paired FRAP experiments would be different. However, we failed to detect any differences in tracer transport rates with or without the presence of vascular pressure. Based on the pulse pressure measured in jugular vein (10 mmHg at 10 Hz), theoretical analysis showed that the blood pressure-driven convection was at least one order of magnitude smaller than diffusion for both small and large molecules [42]. It was concluded that, despite the extreme importance of vasculature in bone physiology, vascular pressure itself does not enhance acute solute transport within the bone LCS [42].

3. PERICELLULAR MATRIX (PCM) IN THE LCS: IMAGING AND QUANTIFICATION OF STRUCTURE AND COMPOSITION

3.1. Early visualization of PCM by transmission electron microscopy (TEM)

Ten years after the publication of the groundbreaking paper by Weinbaum and coworkers [27], definitive proofs of the existence of the PCM, and, in particularly, the transverse tethering fibers within the canalicular channels, were obtained by Schaffler and coworkers [47]. Using intra-cardiac perfusion of ruthenium III hexamine trichloride to stabilize osteocyte PCM for transmission electron microscopy (TEM) imaging, they demonstrated that i) a fiber matrix fills in the pericellular space in the lacunae and canaliculi, ii) transverse tethering elements/fibers span the 80 nm gap in canaliculi, and iii) the tethering fibers connect the osteocyte cell membrane and the canalicular wall with an average spacing of 40 nm [47]. This spacing is much larger than the 7 nm spacing originally hypothesized by Weinbaum et al. [27] and the 7–12 nm PCM cut-off size estimated from tracer perfusion studies as detailed in Section 2.2 (Table 1). This inconsistency may be due to the samples' lengthy and destructive TEM preparation processes, during which artifacts including the loss and/or collapse of PCM fibers might have occurred, resulting in an under-estimation of the

fiber spacing. Thus, it would be more advantageous to probe the structure and function of the PCM *in situ* using minimally invasive methods.

3.2. In situ probing of PCM structure in intact bone

In situ measurements of PCM fiber density were successful achieved by our group using the FRAP-based velocimetry in combination of hydrodynamic modeling of molecular sieving [43]. In this method, one small tracer (sodium fluorescein, 0.45nm radius) is injected in mice and its velocity in mechanically loaded mouse tibia be quantified using paired FRAP tests as briefed in Section 2.4. Due to the small size of sodium fluorescein and its negligible interactions with the PCM fibers, its velocity would represent the velocity of bulk fluid under loading. A larger tracer (parvalbumin, 2.6 nm diameter) is then injected to mice and its velocity measured in the murine tibiae under the same mechanical loading conditions as for the small tracer. The velocity of parvalbumin is typically smaller than that of sodium fluorescein, from which the reflection coefficient ($\sigma = 1\text{-}v_{solute}/v_{fluid}$), an index of PCM's sieving effect on the large tracer is obtained. The reflection coefficient of the PCM to pavalbumin was found to be 8.4% and 5.7% for young (20–22-week-old) and 12–13-month-old B6 male mice, respectively [35, 43].

The molecular sieving of periodically arranged PCM fibers on finite-sized solutes is theoretically modeled as the reduction of the bulk solute flux relative to the fluid flux [43]. In the model, the periodic fluid fields around the fibers arranged in either parallel with or perpendicular to the fluid flow direction are first obtained to calculate fluid flux, while steric exclusion between spherical solutes and the cylindrical fibers is considered in the calculation of solute flux. A close-form solution of the reflection coefficient is thus derived as a function of solute size, fiber size, and fiber spacing (equations 1–3 in [43]). Given the PCM fiber diameter (4 nm, explained in the Section 3.3) and the diameter of parvalbumin (2.6 nm), the average fiber spacing in the PCM can be readily estimated from the experimentally measured reflection coefficients, which was 10.3 nm and 13.4 nm for the young and aged mice, respectively [35]. The reflection coefficient is anticipated to increase non-linearly towards 100% as solute size approaches the fiber spacing, which agreed well with the cut-off behavior (size 7–12 nm) demonstrated from tracer perfusion studies (Table 1, Section 2.2).

The most important advantage of these *in situ* measurements, compared with previous TEM observations, was the freshly sacrificed intact bones being used in the study to eliminate the need of tedious TEM sample preparation processes. However, the assumptions used to develop the molecular sieving model should also be noted as limitations, including the highly idealized PCM fibers and the steric exclusion being the dominant solute-fiber interaction [43]. In our FRAP studies performed in live animals, a significant tracer immobile fraction (17%) was observed in osteocyte lacunae, indicating that some exogenous tracers might have bound to PCM due to either charge, hydrophilic/hydrophobic, or chemical interactions [42]. These interactions, as the solutes of interest become larger, could become increasingly significant and should be considered in future models. Knowledge of the chemical identities of the osteocyte PCM will help our understanding of the complex interactions between the solutes and PCM fibers.

3.3. Perlecan/HSPG2 as a critical component of the osteocyte PCM

Despite the direct visualization of electron-dense fiber matrix and the tethering fibers in the LCS [47], chemical identities of the osteocyte PCM had remained elusive until 2011 when perlecan/HSPG2 was first identified by M.C. Farach-Carson's group [48]. Perlecan/HSPG2 (heparan sulfate proteoglycan 2) is a large proteoglycan found in basement membrane and pericellular matrices [49]. Consisting of five domains and four heparin sulfate (HS) sidechains, perlecan is capable of interacting with many growth factors and extracellular matrix components and controlling tissue interfaces and cell-matrix interactions [50]. Farach-Carson and coworkers confirmed that perlecan is an essential structural component of the osteocyte PCM, through immunohistochemistry staining and immunogold TEM imaging of adult murine cortical LCS [48]. Furthermore, the Farach-Carson group probed both the molecular structure and mechanical properties of isolated, full-length human perlecans using high-resolution atomic force microscopy (AFM) [51]. Their AFM imaging revealed that the core protein of perlecan is long enough to span the pericellular space (~80 nm) in canaliculi [47] with a measured end-to-end length of 170 ± 20 nm and a diameter of ~4 nm [51]. This diameter is chosen to calculate the fiber spacing described in the preceding section 3.2. The AFM pulling experiments showed a strong perlecan core that can withstand ~150 pN of tension, which is ~10 fold higher than the drag force that the transverse fibers experience under physiological 400 με loading [51]. Taken together, these studies demonstrated that perlecan is a component of the osteocyte PCM and perlecan's mechanical properties make it a good candidate of tethering fibers that have been hypothesized [27] to be present and visualized [47] in the LCS.

The importance of perlecan in the osteocytic PCM was further confirmed by TEM imaging of the osteocyte LCS from the C1532Yneo mice, a transgenic model developed to recapitulate the reduced perlecan expression associated with Schwartz-Jampel Syndrome [52]. These perlecan-deficient (hypomorphic [Hypo]) mice exhibited a significant decrease in perlecan secretion [52], and a decreased number of tethering elements per canaliculus (−35%) [48], and narrower pericellular fluid area in the canaliculi (−18% to −55%) [35, 48, 53]. Using the FRAP-based velocimetry, we quantified the reflection coefficient of the PCM in the 12–13-month-old Hypo mice to be 3.9%, which was much lower than those in the age-matched control mice (5.7%) [35] and young control mice (8.4%) [43]. Assuming the fiber diameter to be that of perlecan (4 nm) [51], the effective fiber spacing in Hypo PCM was estimated to be 17.4 nm, in comparison with the 13.4 nm and 10.3 nm for the age-matched control and young control PCM, respectively [35]. The sparser fibers in the Hypo PCM led to a significant reduction (−35%) in the fluid drag force that the osteocytes experienced during physiologically loading. This reduced stimulation to osteocytes might account for the diminished bone formation observed in the Hypo mice when they were subjected to *in vivo* unilateral tibial loading (8.5 N, 4 cycles/sec, 5 min per session, 5 sessions over 10 days) that elicited robust bone formation in normal control mice [35]. Similarly, the decrease of the PCM fiber density in aged mice (fiber spacing 13.4 nm) relative to that in young adult mice (fiber spacing 10.3 nm) is anticipated to reduce fluid drag force, in agreement with the decreased responsiveness of aging skeleton to *in vivo* loading [54].

Taken together, these studies demonstrate that the osteocyte PCM is not a static entity and the PCM fiber density varies with aging and perlecan deficiency. These PCM variations may impact the immediate environment of osteocytes. As for fluid transport, a sparser PCM with a larger fiber spacing is associated with lower hydraulic resistance, higher fluid velocity, increased fluid sheer stress, but decreased fluid drag force and thus reduced mechanosensitivity of the osteocytes to mechanical loading [35]. However, for solute transport, a sparser PCM is associated with a reduced molecular sieving effect and elevated diffusion and convection of both small (sodium fluorescein) and large tracers (parvalbumin) as demonstrated in the Hypo PCM (diffusion: +33%, +40%; convective velocity: +39%, 42%) [35]. Although the consequences of a sparser PCM on fluid/solute transport in the LCS become clearer, the detailed biological effects at the cellular and molecular levels that eventually lead to the attenuated *in vivo* bone formation have not been determined yet.

3.4. Future directions: unresolved questions

Despite the recent advances as reviewed above, our understanding on the osteocyte PCM remains quite limited. For examples, besides perlecan, we do not know what other components are present in the PCM and how they interact with each other, with cell membrane, and with canalicular wall. Due to the relatively small volume occupied by the osteocyte PCM (~10% volume fraction) [21, 53, 55] and its ultra-thin thickness (~80 nm) [47, 53], quantitative interrogation of the osteocyte PCM remains extremely difficult with current technologies. To overcome this challenge, our group recently applied orthogonal click chemistry and labeled newly synthesized osteocyte PCM *in vivo* and *in vitro*, which were isolated and enriched from the extensive ECM background, with the goal of elucidating the PCM components via mass spectroscopy [56]. Another question is the turnover rate of the osteocyte PCM. In adult skeleton, the mineralized ECM is usually quite stable and only undergoes matrix remodeling through osteoclastic resorption in cases of repairing matrix damage [2], fracture healing [57], or removing minerals during reproduction [58]. In comparison, the osteocyte PCM is likely to be more dynamic due to new findings that osteocytes are actively involved in peri-lacunar and peri-canalicular remodeling by secreting various MMPs and forming acidic environments during reproduction [59–61]. These factors may also degrade the osteocyte PCM and change the local composition and structure of the PCM. Furthermore, time lapse imaging from Dallas's group showed that newly embedded osteoid osteocytes exhibit noticeable motile cell body and cell processes within the LCS [62]. It is to be determined whether the osteocyte PCM would be deformed or slide over the cell dendrite and the canalicular wall. The mechanisms by which osteocyte PCM interacts with the dendrite membrane and mineralized canalicular wall are poorly understood. Although smooth canalicular surface was typically assumed in most theoretical models [27–29, 45], a recent study using ultra high voltage electron microscopy showed a high roughness of the canalicular wall and an irregular, non-uniform pericellular fluid gap in human canaliculi [63]. How osteocyte PCM bridges the irregular gap between cell membrane and canalicular wall is an issue to be resolved. Lastly, as mechanical loading induces significant fluid flow through the PCM that may activate osteocytes [27], one may ask whether mechanical loading influences the synthesis and turnover of the PCM through direct actions on osteocytes or indirect flow induced shedding of the PCM fibers. Future investigations are needed to obtain a more comprehensive

understanding of the PCM composition, turnover, potential regulators, and its interactions with cell membrane and calcified bone matrix.

4. CONCLUSIONS

The submicron-thin PCM residing in the LCS channels serves as bone's natural chromatography column and controls both solute transport through the bone matrix (Fig. 1). Osteocyte PCM forms an important microenvironment for osteocytes, the most abundant cells and primary mechanosensors in bone, and plays many roles in bone mechanosensing, cell-cell signaling, osteocyte viability, and drug delivery. Despite the progress in elucidating the sieving and mechanical properties of PCM using cutting-edge imaging/engineering/modeling approaches, there are still many unknowns about PCM. Because osteocytes are capable of modifying their immediate environment where PCM is occupied, it is important to know how the osteocyte PCM is altered during bone development and aging, under mechanical loading or disuse, and in both physiological and pathological conditions. Elucidating the composition and turnover dynamics of the osteocyte PCM will lead to better understanding of PCM-cell interactions. Being a critical interface between osteocytes and their extracellular environment, PCM holds the key to unlock the secrets how to precisely regulate osteocyte functions and bone remodeling in order to promote bone health in clinical applications.

Acknowledgments

L Wang received grant support from the National Institutes of Health (R01AR054385).

References

Papers of particular interest, published recently (within 5 years), have been highlighted as:

* of importance

** of major importance

1. Bonewald LF. The amazing osteocyte. J Bone Miner Res. 2011; 26(2):229–38. [PubMed: 21254230]

2*. Schaffler MB, et al. Osteocytes: master orchestrators of bone. Calcif Tissue Int. 2014; 94(1):5–24. Provided a comprehensive review on osteocyte cell-cell signaling in repairing tissue damage and remodeling. [PubMed: 24042263]

3. Weinstein RS, et al. Inhibition of osteoblastogenesis and promotion of apoptosis of osteoblasts and osteocytes by glucocorticoids. Potential mechanisms of their deleterious effects on bone. J Clin Invest. 1998; 102(2):274–82. [PubMed: 9664068]

4. Busse B, et al. Decrease in the osteocyte lacunar density accompanied by hypermineralized lacunar occlusion reveals failure and delay of remodeling in aged human bone. Aging Cell. 2010; 9(6): 1065–75. [PubMed: 20874757]

5. Qiu S, et al. Reduced iliac cancellous osteocyte density in patients with osteoporotic vertebral fracture. J Bone Miner Res. 2003; 18(9):1657–63. [PubMed: 12968675]

6. Piekarski K, Munro M. Transport mechanism operating between blood supply and osteocytes in long bones. Nature. 1977; 269(5623):80–2. [PubMed: 895891]

7. Fritton SP, Weinbaum S. Fluid and Solute Transport in Bone: Flow-Induced Mechanotransduction. Annu Rev Fluid Mech. 2009; 41:347–374. [PubMed: 20072666]

8. McClung MR, et al. Romosozumab in postmenopausal women with low bone mineral density. N Engl J Med. 2014; 370(5):412–20. [PubMed: 24382002]

9. Dallas SL, Prideaux M, Bonewald LF. The osteocyte: an endocrine cell … and more. Endocr Rev. 2013; 34(5):658–90. [PubMed: 23612223]

10. Franz-Odendaal BK, Hall TA, Witten PE. Buried alive: how osteoblasts become osteocytes. Dev Dyn. 2006; 235(1):176–90. [PubMed: 16258960]

11. Winkler DG, et al. Osteocyte control of bone formation via sclerostin, a novel BMP antagonist. EMBO J. 2003; 22(23):6267–76. [PubMed: 14633986]

12. Zhao S, et al. MLO-Y4 osteocyte-like cells support osteoclast formation and activation. J Bone Miner Res. 2002; 17(11):2068–79. [PubMed: 12412815]

13. Xiong J, et al. Matrix-embedded cells control osteoclast formation. Nat Med. 2011; 17(10):1235–41. [PubMed: 21909103]

14. You L, et al. Osteocytes as mechanosensors in the inhibition of bone resorption due to mechanical loading. Bone. 2008; 42(1):172–9. [PubMed: 17997378]

15. Duan P, Bonewald LF. The role of the wnt/beta-catenin signaling pathway in formation and maintenance of bone and teeth. Int J Biochem Cell Biol. 2016; 77(Pt A):23–9. [PubMed: 27210503]

16. Riquelme MA, et al. Mitogen-activated Protein Kinase (MAPK) Activated by Prostaglandin E2 Phosphorylates Connexin 43 and Closes Osteocytic Hemichannels in Response to Continuous Flow Shear Stress. J Biol Chem. 2015; 290(47):28321–8. [PubMed: 26442583]

17. de Castro LF, et al. VEGF Receptor 2 (VEGFR2) Activation Is Essential for Osteocyte Survival Induced by Mechanotransduction. J Cell Physiol. 2015; 230(2):278–85. [PubMed: 25102966]

18. Kitase Y, et al. Mechanical induction of PGE2 in osteocytes blocks glucocorticoid-induced apoptosis through both the beta-catenin and PKA pathways. J Bone Miner Res. 2010; 25(12): 2657–68. [PubMed: 20578217]

19. Zeng Y, Cowin SC, Weinbaum S. A fiber matrix model for fluid flow and streaming potentials in the canaliculi of an osteon. Ann Biomed Eng. 1994; 22(3):280–92. [PubMed: 7978549]

20. Burger EH, Klein-Nulend J. Mechanotransduction in bone--role of the lacuno-canalicular network. FASEB J. 1999; 13(Suppl):S101–12. [PubMed: 10352151]

21. Cardoso L, et al. Advances in assessment of bone porosity, permeability and interstitial fluid flow. J Biomech. 2013; 46(2):253–65. [PubMed: 23174418]

22. Cowin SC. Bone poroelasticity. J Biomech. 1999; 32(3):217–38. [PubMed: 10093022]

23. Dyke JP, Aaron RK. Noninvasive methods of measuring bone blood perfusion. Ann N Y Acad Sci. 2010; 1192:95–102. [PubMed: 20392223]

24*. Granke M, Does MD, Nyman JS. The Role of Water Compartments in the Material Properties of Cortical Bone. Calcif Tissue Int. 2015; 97(3):292–307. Provided a review on bound water and free water distribution in bone tissue and their roles in bone material properties. [PubMed: 25783011]

25. Aarden EM, Burger EH, Nijweide PJ. Function of osteocytes in bone. J Cell Biochem. 1994; 55(3): 287–99. [PubMed: 7962159]

26. Pienkowski D, Pollack SR. The origin of stress-generated potentials in fluid-saturated bone. J Orthop Res. 1983; 1(1):30–41. [PubMed: 6679573]

27. Weinbaum S, Cowin SC, Zeng Y. A model for the excitation of osteocytes by mechanical loading-induced bone fluid shear stresses. J Biomech. 1994; 27(3):339–60. [PubMed: 8051194]

28. Cowin SC, Weinbaum S, Zeng Y. A case for bone canaliculi as the anatomical site of strain generated potentials. J Biomech. 1995; 28(11):1281–97. [PubMed: 8522542]

29. You L, et al. A model for strain amplification in the actin cytoskeleton of osteocytes due to fluid drag on pericellular matrix. J Biomech. 2001; 34(11):1375–86. [PubMed: 11672712]

30. Wang Y, et al. A model for the role of integrins in flow induced mechanotransduction in osteocytes. Proc Natl Acad Sci U S A. 2007; 104(40):15941–6. [PubMed: 17895377]

31. Han Y, et al. Mechanotransduction and strain amplification in osteocyte cell processes. Proc Natl Acad Sci U S A. 2004; 101(47):16689–94. [PubMed: 15539460]

32. Webster DJ, et al. Studying osteocytes within their environment. Bone. 2013; 54(2):285–95. [PubMed: 23318973]

33. Li W, et al. The dependency of solute diffusion on molecular weight and shape in intact bone. Bone. 2009; 45(5):1017–23. [PubMed: 19647808]

34. Price C, et al. Real-time measurement of solute transport within the lacunar-canalicular system of mechanically loaded bone: direct evidence for load-induced fluid flow. J Bone Miner Res. 2011; 26(2):277–85. [PubMed: 20715178]

35**. Wang B, et al. Perlecan-containing pericellular matrix regulates solute transport and mechanosensing within the osteocyte lacunar-canalicular system. J Bone Miner Res. 2014; 29(4): 878–91. Quantified diffusion and convection in perlecan deficient bone, measured reflection coefficient of PCM of normal and decreased perlecan expression, and determined the effective fiber spacing for the PCM. Linked cellular hydraulic forces (shear and drag) with in vivo bone formation and provided evidence that perlecan serves as a flow sensor in the LCS. [PubMed: 24115222]

36. Wang L, et al. In situ measurement of solute transport in the bone lacunar-canalicular system. Proc Natl Acad Sci U S A. 2005; 102(33):11911–6. [PubMed: 16087872]

37. Wang L, et al. Delineating bone's interstitial fluid pathway in vivo. Bone. 2004; 34(3):499–509. [PubMed: 15003797]

38. Tami AE, Schaffler MB, Knothe Tate ML. Probing the tissue to subcellular level structure underlying bone's molecular sieving function. Biorheology. 2003; 40(6):577–90. [PubMed: 14610309]

39*. Ciani C, et al. Ovariectomy enhances mechanical load-induced solute transport around osteocytes in rat cancellous bone. Bone. 2014; 59:229–34. Provided evidence that estrogen deficiency altered solute perfusion in cortical and trabecular bone. [PubMed: 24316418]

40. Lang SB, Stipanich N, Soremi EA. Diffusion of glucose in stressed and unstressed canine femur in vitro. Ann N Y Acad Sci. 1974; 238:139–48. [PubMed: 4531258]

41. Fernandez-Seara MA, Wehrli SL, Wehrli FW. Diffusion of exchangeable water in cortical bone studied by nuclear magnetic resonance. Biophys J. 2002; 82(1 Pt 1):522–9. [PubMed: 11751339]

42. Li W, et al. Does blood pressure enhance solute transport in the bone lacunar-canalicular system? Bone. 2010; 47(2):353–9. [PubMed: 20471508]

43**. Wang B, et al. Quantifying load-induced solute transport and solute-matrix interaction within the osteocyte lacunar-canalicular system. J Bone Miner Res. 2013; 28(5):1075–86. Developed the FRAP-based velocimetry to quantify reflection coefficient of the PCM and the molecular sieving model to derive the effective fiber spacing. [PubMed: 23109140]

44. Knothe Tate ML, Knothe U. An ex vivo model to study transport processes and fluid flow in loaded bone. J Biomech. 2000; 33(2):247–54. [PubMed: 10653041]

45. Zhou X, Novotny JE, Wang L. Modeling fluorescence recovery after photobleaching in loaded bone: potential applications in measuring fluid and solute transport in the osteocytic lacunar-canalicular system. Ann Biomed Eng. 2008; 36(12):1961–77. [PubMed: 18810639]

46. Hillsley MV, Frangos JA. Bone tissue engineering: the role of interstitial fluid flow. Biotechnol Bioeng. 1994; 43(7):573–81. [PubMed: 11540959]

47. You LD, et al. Ultrastructure of the osteocyte process and its pericellular matrix. Anat Rec A Discov Mol Cell Evol Biol. 2004; 278(2):505–13. [PubMed: 15164337]

48. Thompson WR, et al. Perlecan/Hspg2 deficiency alters the pericellular space of the lacunocanalicular system surrounding osteocytic processes in cortical bone. J Bone Miner Res. 2011; 26(3):618–29. [PubMed: 20814969]

49. Iozzo RV, et al. The biology of perlecan: the multifaceted heparan sulphate proteoglycan of basement membranes and pericellular matrices. Biochem J. 1994; 302(Pt 3):625–39. [PubMed: 7945186]

50*. Farach-Carson MC, et al. Border patrol: insights into the unique role of perlecan/heparan sulfate proteoglycan 2 at cell and tissue borders. Matrix Biol. 2014; 34:64–79. Provided a comprehensive review on perlecan's structural and biological functions along various tissue interfaces including bone LCS. [PubMed: 24001398]

51**. Wijeratne SS, et al. Single molecule force measurements of perlecan/HSPG2: A key component of the osteocyte pericellular matrix. Matrix Biol. 2016; 50:27–38. AFM imaging of the

dimensions of isolated human perlecan and tested the mechanical strength of the perlecan core proteins by AFM pulling experiments. [PubMed: 26546708]

52. Rodgers KD, et al. Reduced perlecan in mice results in chondrodysplasia resembling Schwartz-Jampel syndrome. Hum Mol Genet. 2007; 16(5):515–28. [PubMed: 17213231]

53*. Lai X, et al. The dependences of osteocyte network on bone compartment, age, and disease. Bone Res. 2015; 3 Investigated the variations of the LCS in murine bone and discovered the relatively constant of the canalicular number density per unit lacunar surface.

54. Lynch ME, et al. Tibial compression is anabolic in the adult mouse skeleton despite reduced responsiveness with aging. Bone. 2011; 49(3):439–46. [PubMed: 21642027]

55*. Fan L, et al. A multiscale 3D finite element analysis of fluid/solute transport in mechanically loaded bone. Bone Res. 2016; 4:16032. Modeling fluid and solute transport at three levels (whole bone, lacunar, and canalicular levels). [PubMed: 27722020]

56. Martinez, JR., Pei, S., Wang, L. Annual meeting of American Association for Bone and Mineral Research. Denver, CO: 2017. Profiling the composition of osteocyte pericellular matrix (PCM) in vivo and in vitro.

57. Marsell R, Einhorn TA. The biology of fracture healing. Injury. 2011; 42(6):551–5. [PubMed: 21489527]

58. Topping J, et al. Osteoporosis in pregnancy: more than postural backache. Prof Care Mother Child. 1998; 8(6):147–50. [PubMed: 10197021]

59**. Jahn K, et al. Osteocytes Acidify Their Microenvironment in Response to PTHrP In Vitro and in Lactating Mice In Vivo. J Bone Miner Res. 2017; 32(8):1761–1772. New evidence that osteocytes are capable of remodeling the surrounding matrix. [PubMed: 28470757]

60**. Nango N, et al. Osteocyte-directed bone demineralization along canaliculi. Bone. 2016; 84:279–88. New evidence that osteocytes are capable of remodeling the surrounding matrix. [PubMed: 26709236]

61. Qing H, et al. Demonstration of osteocytic perilacunar/canalicular remodeling in mice during lactation. J Bone Miner Res. 2012; 27(5):1018–29. [PubMed: 22308018]

62. Dallas SL, Bonewald LF. Dynamics of the transition from osteoblast to osteocyte. Ann N Y Acad Sci. 2010; 1192:437–43. [PubMed: 20392270]

63**. Kamioka H, et al. Microscale fluid flow analysis in a human osteocyte canaliculus using a realistic high-resolution image-based three-dimensional model. Integr Biol (Camb). 2012; 4(10): 1198–206. Irregular canalicular wall and rough surface were observed and osteocyte cell processes appeared not in direct contact with canalicular wall under 2.2 nm resolution. [PubMed: 22858651]

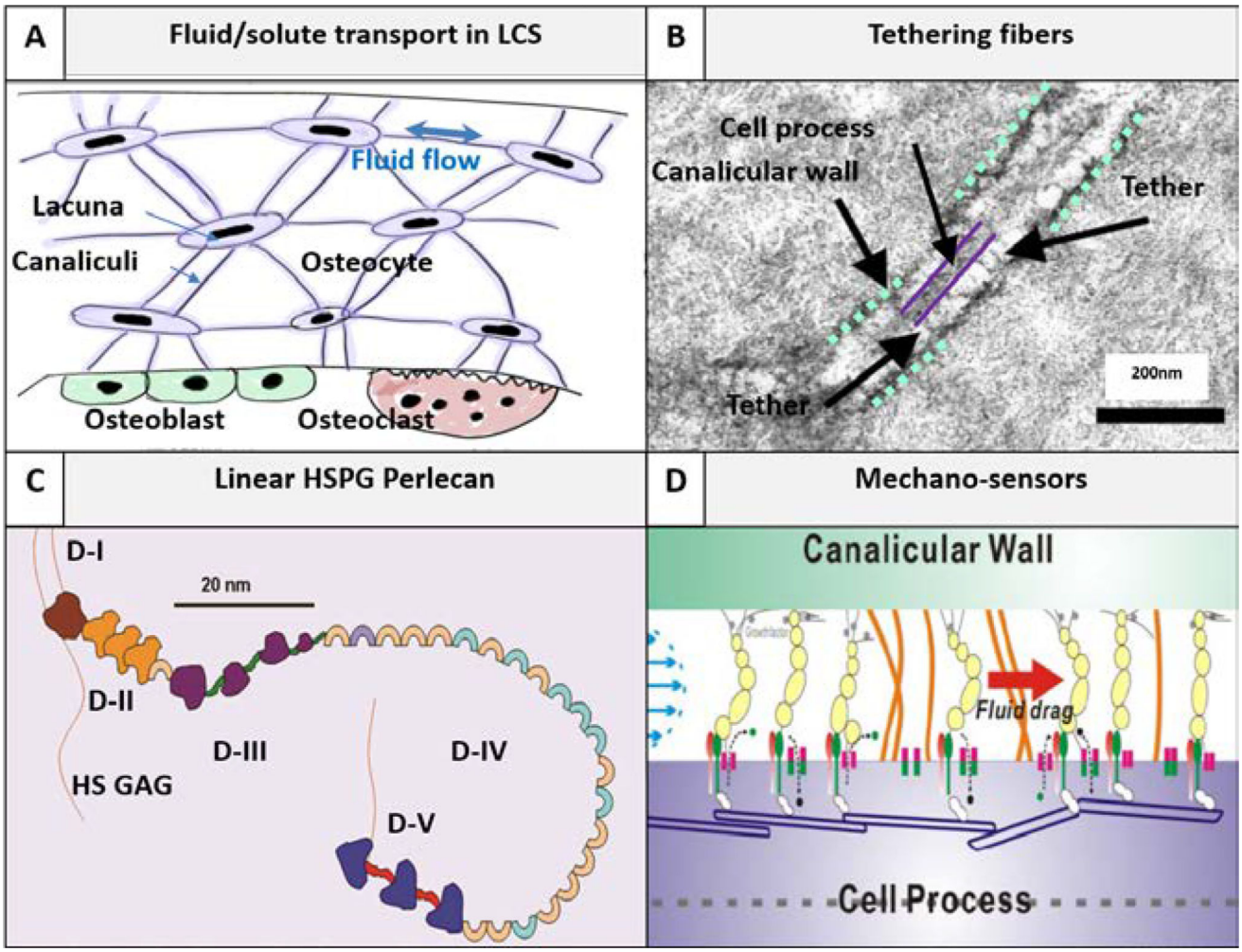

Fig. 1.

Pericellular matrix (PCM)-filled lacunar-canalicular system (LCS) is bone's natural chromatographic column, where fluid/solute transport to and from osteocytes is regulated. (A) Fluid and solute transport in the LCS is critical for osteocyte survival (e.g., nutrient supply and cell-cell signaling) and proper function (e.g., mechanosensing) [7]. (B) The canalicular channel contains an electron-dense PCM and transverse fibers tether the cell process with the canalicular wall as seen under transmission electron microscopy [47]. (C) Schematic of perlecan/HSPG2, a proteoglycan, consisting of five domains and four HS sidechains (Courtesy of M.C. Farach-Carson). Perlecan is the first identified PCM component [48] with a contour length of 170 nm and diameter of ~4 nm [51]. (D) Perlecan as well as other tethering fibers regulate the fluid and solute transport in the LCS. The PCM fiber density (inversely related to fiber spacing) determines the LCS's hydraulic permeability, the magnitude of fluid velocity and the fluid drag force so that osteocytes can sense and respond to mechanical loading [43]. The PCM fiber density also modulates solute diffusion and convection due to steric exclusion between finite sized solutes and the PCM fibers [35]. The osteocyte PCM fiber spacing is found to be 10.3, 13.4, 17.4 nm in young adult, aged, and aged perlecan deficient LCS, respectively [35].

Table 1

Summary of selective in vivo tracer studies on the LCS's cut-off size and tracer diffusivity

Tracer	MW (kDa)	Dia (nm)	Animal/circulation time/sample preparation [reference]	Penetration to LCS	Diffusivity D_{LCS} ($\mu m^2/s$)	Characteristic time t_c (sec)#
Sodium fluorescein	0.4	0.9	4–6-month-old B6 female mice/20 min/ intact bone [36]	Yes	330 ± 60	68
Sodium fluorescein	0.4	0.9	3–5-month-old B6 mice/tail vein/30 min/in situ imaging of intact bone [33]	Yes	294.8 ± 45.8	77
Sodium fluorescein	0.4	0.9	3–4-month-old B6 male mice/tail vein/30 min/in situ imaging of intact bone [34]	Yes	272	83
Sodium fluorescein	0.4	0.9	12–13-month-old B6 male mice/tail vein/30 min/in situ imaging of intact bone [35]	Yes	302 ± 72	75
Reactive red	1.47	1.6	2–3-month-old Sprague-Dawley male rats/jugular vein/5 min/decalcified sections [37]	yes	-	
Micro-peroxidase	1.86	1.7	2–3-month-old Sprague-Dawley male rats/jugular vein/5 min/decalcified sections [37]	yes	-	
Dextran	3	2.8*	3–5-month-old B6 mice/ tail vein/1.5h/in situ imaging of intact bone [33]	yes	128.0 ± 31.7	176
Dextran	3	2.8*	Skeletal matured Sprague-Dawley female rats/tail vein/1–2min/plastic embedded sections [38]	yes	-	
Dextran	10	4.6*	3–5-month-old B6 mice/ tail vein/3h/in situ imaging of intact bone [33]	Yes (no load)	0**	-
Dextran	10	4.6*	Skeletal matured Sprague-Dawley female rats/tail vein/1–2min/plastic embedded sections [38]	No (no load) Yes (3000 με)	-	
parvalbumin	12.3	2.6	3–5-month-old B6 mice/tail vein/1.5h/in situ imaging of intact bone [33]	yes	157.4 ± 87.7	143
parvalbumin	12.3	2.6	12–13-month-old B6 male mice/tail vein/2h/in situ imaging of intact bone [35]	yes	200 ± 55	113
Horseradish peroxidase	40	6	2–3-month-old Sprague-Dawley male rats/jugular vein/5 min/decalcified sections [37]	yes	-	
ovalbumin	43	6	3–5-month-old B6 mice/tail vein/7h/in situ imaging of intact bone [33]	yes	65.3 ± 20.7	346
albumin	67	7	5-month-old Sprague-Dawley female rats/jugular vein/4–5min/plastic sections [39]	Yes (no load) Yes (500 με)	-	
dextran	70	12*	Skeletal matured Sprague-Dawley female rats/tail vein/1–2min/plastic embedded sections [38]	No (no load) No (3000 με))	-	
ferritin	440	12	2–3-month-old Sprague-Dawley male rats/jugular vein/5 min/decalcified sections [37]	No	-	

Notes:

#Characteristic time was calculated as $t_C = R^2/D$ for molecular diffusion over a representative osteon of radius R = 150 μm;

*Stokes diameter was estimated for these linear dextran molecules https://www.sigmaaldrich.com/content/dam/sigma-aldrich/docs/Sigma/Product_Information_Sheet/1/fd250spis.pdf

**dextran 10 kDa was perfused in bone but no fluorescence recovery was observed during the ~5 min imaging period after photobleaching.

Table 2

Measurements of convective velocity of solutes in the canalicular channels of mechanically loaded tibiae

Solute /MW	Animal age/sex/species	Peak load/surface strain/frequency	Peak velocity (μm/s)	Characteristic time t_c (sec)*
Sodium fluorescein/376Da	3–4-month-old B6 male mice	2.8 N/477 με/0.5 Hz	53.9 [34]	2.8
Sodium fluorescein/376Da	12–13-month-old B6 male mice	2.8 N/306 με/0.5 Hz	51.1 [35]	2.9
Parvalbumin/12.3kDa	20–22 week-old B6 male mice	4.8 N/510/0.5 Hz	55.8 [43]	2.7
Parvalbumin/12.3kDa	20–22 week-old B6 male mice	2.8 N/298/0.5 Hz	43.1 [43]	3.5
Parvalbumin/12.3kDa	12–13-month-old B6 male mice	2.8 N/306 με/0.5 Hz	48.2 [35]	3.1
Parvalbumin/12.3kDa	20–22 week-old B6 male mice	2.8 N/298/1 Hz	33.3 [43]	4.5
Parvalbumin/12.3kDa	20–22 week-old B6 male mice	2.8 N/298/2 Hz	28.5 [43]	8.8

Note:

*The characteristic transport time ($t_C = R_C / V_S$) is calculated for a representative osteon (R_C =150 μm).